THE ROLE OF THE OXIDE IN THE CARRIER SELECTIVITY OF METAL/POLY-SI/OXIDE CONTACTS TO SILICON WAFERS

G.J.M. Janssen* (janssen@ecn.nl), M.K. Stodolny, I.G. Romijn, L.J. Geerligs
ECN Solar Energy, P.O. Box 1, NL-1755 ZG Petten, The Netherlands
*Phone: +31 88 515 4803

ABSTRACT: Simulation results are presented that elucidate the role of the interfacial oxide layer in the passivation and carrier selectivity exhibited by doped poly-Si contact layers. An approach is introduced by which the oxide is represented as a layer with limited charge carrier mobility. This approach is easy to implement in numerical simulations and directly affects the conductivity of minority as well as of majority charge carriers, which determine the carrier selectivity. Our results show that for optimal passivation and carrier selectivity the oxide should not be a perfect tunnel oxide but should show higher effective charge carrier mobility. This means that poly-Si/oxide layers with substantial in-diffusion tails can be used, which has benefits when fire-through metallization is applied.
Keywords: contact, passivation, carrier selectivity, simulation, silicon solar cell.

1 INTRODUCTION

Effective carrier selective contact layers can be made by deposition of highly-doped poly-Si on an interfacial oxide grown on the c-Si wafer [1-3]. Carrier selectivity is provided by an asymmetrical conductivity, which enhances the transport of one carrier to the contact and suppresses the other [4]. The high dopant concentrations in the poly-Si are the basis for the carrier selectivity of the poly-Si/oxide contact layers. The interfacial oxide is a diffusion barrier for dopants like phosphorous and boron, which means that in the poly-Si layer uniform dopant concentrations close to the solubility level can be obtained [3,5,6]. But, as experimental and theoretical studies have indicated, the presence of the thin interfacial oxide layer also has a function in the reduction of the contact recombination parameter J_{0c} [5-8].

It has been assumed that the oxide layer is a barrier for charge carrier transport to the metal. An effective suppression of the minority carrier transport will reduce the J_{0c}; at the same time this barrier should not significantly impede majority carrier transport, i.e. lead not to a high contact resistance ρ_c. It has been recognized that the key for a good carrier selective contact is a good balance between the recombination properties and contact resistance [4,9].

Another contribution to the contact recombination will come from the recombination at the surface of the wafer. It is well known that interfacial oxides grown either thermally or in a wet-chemical process contribute to improved surface passivation by reduction of the density of interface states (D_{it}). Hydrogenation further reduces the D_{it}. Most passivation schemes for Si-surfaces also include a field or band-bending effect, i.e. by applying fixed charges at the surface the concentration of minority carriers is reduced. In the poly-Si/oxide contacts, the highly-doped poly-Si layer presents the field effect.

In this paper we will first consider first the wafer passivation and its relation with the dopant concentration in the poly-Si, the thickness of interfacial oxide and the D_{it}, or alternatively the surface recombination parameter S_{int}, to which it is proportional.

Next, we consider in more detail the importance of the charge carrier transport by the oxide. Experimental data suggest that properties like thickness, homogeneity, impurity level of the oxide depend very much on the processing conditions [5-7,10]. Different assumptions on the nature of the oxide have already led to two very different physical models for the oxide, i.e. as a quantum-mechanical tunnel barrier [11], or as layer of pin-holes causing current constriction [6,12].

Here we will present numerical simulations in which we represent the oxide either as a quantum-mechanical tunnel or by a thin silicon layer with limited charge carrier mobility. It will be shown that for very low effective charge carrier mobility these models give similar results, but that the oxide with the optimal (J_{0c}, ρ_c) has an effective mobility higher than that of a perfect quantum-mechanical tunnel oxide. Moreover, experimental data suggest such a higher effective mobility is more representative for the carrier transport through the oxide.

2 MODELLING AND SIMULATION DETAILS

2.1 The Girisch model

The Girisch model [13] was used to estimate the band-bending induced in the poly-Si on one side of an insulating oxide and in the c-Si on the other side. The assumptions used by the Girisch model are that the effective charge induced by band-bending is the same in both semiconductors (charge neutrality), that the electrostatic potential is continuous and that the quasi - Fermi levels are constant throughout the system. This latter assumption is only valid if the recombination is not too high. Moreover, band-gap narrowing effects are not included. The oxide is represented by a change in electrostatic potential Ψ:

$$\Delta\Psi = \frac{Qqd}{\epsilon_{SiOx}\epsilon_0} \qquad (1)$$

Here Q is the charge density associated with the bend-bending, d is the thickness of the oxide, ϵ_0 the vacuum permittivity, ϵ_{SiOx} the relative dielectric constant of the oxide (3.9 in this work) and q the elementary charge. Following the approach of ref. [13] the minority carrier density n_s at the oxide/c-Si interface can be calculated for a given splitting of the quasi-Fermi-levels ΔE_F; the recombination parameter J_{0p} characterizing the recombination at this interface is then obtained from:

$$J_{0p} = \frac{qn_sS_{int}}{\exp(q\Delta E_F/kT)} \qquad (2)$$

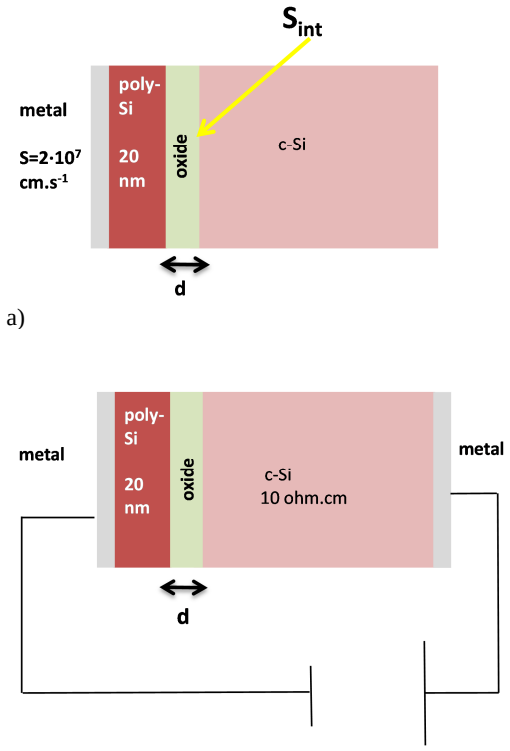

Figure 1: Schematics of the structures used in Atlas simulation to calculate J_{0c} (a) and ρ_c (b).

Here S_{int} is the recombination velocity of the minority carrier at the interface, and k and T are the Boltzmann constant and temperature respectively. At strong enough band-bending (high enough Q) J_{0p} values are independent of the chosen Fermi-level splitting [14].

2.2 Atlas simulations

The schematic structures of Fig. 1 were used to calculate the J_{0c} and ρ_c, with the simulation package Atlas of Silvaco [15]. In this work the polarity of the c-Si and poly-Si was taken the same. For the calculation of J_{0c} in all cases a base dopant concentration of $5 \cdot 10^{14}$ cm^{-3} was assumed, in the calculation of the ρ_c the base resistivity was 10 ohmcm. For the calculation of J_{0c} the metal is represented by a surface with theoretical maximum recombination velocity of $2 \cdot 10^7$ cms^{-1}. The poly-Si thickness was 20 nm, i.e. sufficient to include the band-bending zone. The recombination velocity at the metal surface is so high that the actual lifetime in the poly-Si is not critical. In this work the Shockley-Read-Hall lifetime of the poly-Si was set at a rather high value of 1 µs; in reality it can be as low as 1 ps. The high recombination value assumed at the surface is in fact equivalent to recombination velocity of a 20 nm thick poly-Si layer with a lifetime of 0.1 ps. In the simulation the poly-Si lifetime will only affect the distribution of the recombination between the poly-Si volume and the surface. The charge carrier mobility in poly-Si was set to 14 cm^{2}V^{-1}s^{-1}, in agreement with experimental data [3]. Also this value is not critical for the J_{0c}.

At the interface of the oxide and c-Si a minority recombination rate S_{int} was assumed; in this way J_{0c} includes J_{0p}. In some cases an in-diffusion tail in the c-Si was modelled by a Gaussian profile with a maximum concentration N_s at the oxide/c-Si interface and depth parameter a. The Auger recombination modelled according to ref. [16] and Schenk's band-gap narrowing model [17] were used for both c-Si and poly-Si.

R_{comb} is calculated by summing all recombination at the poly-Si/metal interface, in the poly-Si and at the oxide/wafer interface (R_{comb}) and any tail region present. J_{0c} is then extracted from:

$$qR_{comb} = J_{0c}\frac{\Delta n(N_D+\Delta n)}{n_i^2} \qquad (3)$$

Δn and N_D are the excess and dopant concentration in the base, respectively, and n_i is the intrinsic charge carrier concentration assumed to be $8.6 \cdot 10^9$ cm^{-3}, i.e. the value commonly used when extracting J_0 values from lifetime measurements with the WTC120 Lifetime Tester [18]. At high injection levels J_{0c} becomes independent of Δn, here the value at $\Delta n = 10 \cdot N_D$ will be reported.

The area specific junction resistance ρ_c is calculated from an *IV* curve of the structure in Fig.1b in the range 0-60 mV. Contact resistances between metal and poly-Si and between metal and wafer were set to zero, in practice values < 10 mΩ.cm^2 are expected for this contribution to the total ρ_c.The junction resistance ρ_c is calculated by subtracting the base resistance (0.177 Ω.cm^2 in this work) from the total resistance.

Two approaches were used to represent the oxide:

a) As a SiO_2 tunnel oxide. The effective masses for holes and electrons were set at 0.4 m_0 (m_0 is the electron rest mass). With a SiO_2 bandgap of 8.9 eV the tunnel barrier is about 3.4 eV for electrons and 4.4 eV for holes.

b) As an intrinsic Si layer with thickness 1.5 nm and an effective charge carrier mobility μ that represents the permeability for charge carriers in the oxide. In the present simulation the mobility of holes and electrons was given the same value. Usually electrons are more mobile than holes, but their mobilities are expected to be in the same order of magnitude [9].

2.3 Quokka simulations

Quokka [19] was used to calculate the maximum efficiency possible for a given combination of J_{0c} and ρ_c. To exclude all other factors affecting the efficiency, the base resistivity was set to 10^6 Ωcm and an infinite base lifetime as assumed. All other resistances and recombination parameters were set zero; the generated current density was taken as at 43.3 mAcm^{-2} [20].

3 RESULTS

3.1 Passivation effect

Calculations using the Girisch model as outlined in 2.1 showed that the field of the highly doped polysilicon is very effective in the reduction of the surface recombination of the wafer (Fig. 2). Layers of n+ or p+ poly-Si with dopant concentration > 10^{19} cm^{-3} provide fields that are equivalent to a charge density > 10^{12} cm^2, i.e. of similar magnitude as field provided by the fixed charges of AlO_x or SiN_x. At these high dopant concentrations the results are similar for p+ poly Si layers (not shown). The charges slightly decrease with oxide thickness d, but the effect is not very critical in the range 1-2 nm (Fig. 2b). The thickness of the polysilicon

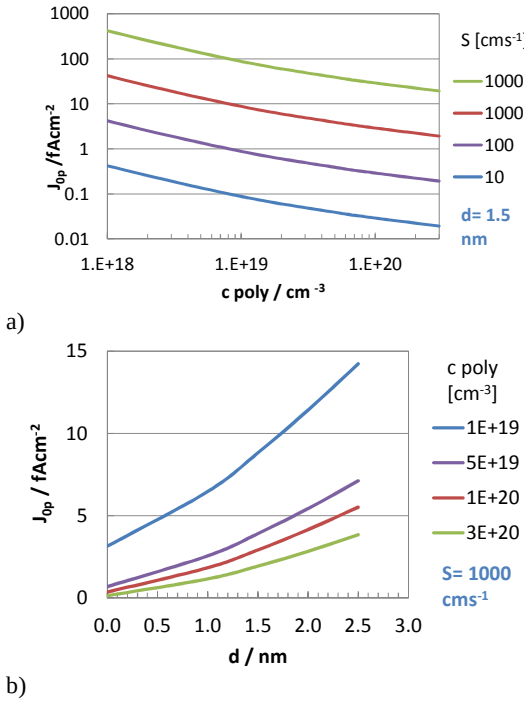

Figure 2: The recombination parameter J_{0p} of the oxide/c-Si interface calculated according to Girisch model a) with a fixed oxide thickness of 1.5 nm as function of the n+-poly dopant concentration, and b) as function of the oxide thickness d.

is even less critical, but it must be larger than the width of the region where band bending occurs, i.e. a few times the Debye length λ. Using $\lambda = \sqrt{\epsilon_{Si}\epsilon_0 kT/(q^2 N_D)}$ we find that λ is ≈ 0.5 nm for poly-Si with doping levels of about N_D=10^{20} cm^{-3} and relative dielectric constant for Si ϵ_{Si}=11.7, which means that poly-Si layers as thin as 5 nm are sufficient to provide the field effect.

A very critical parameter is the S_{int}, which reflects the number of defects at the oxide/c-Si interface. Fig. 2a shows that, within the approximations of the Girisch model, the defect density must be such that S_{int} < 1000 cms^{-1} in order to achieve J_{0p} < 10 fAcm^{-2}.

3.2 Carrier selectivity

In agreement with the results of Steinkemper *et al.* [21], we found that a tunnel oxide is very efficient to suppress the J_{0c} of poly-Si layers (Fig. 3). In all calculations with oxides thickness between 1 and 2 nm we found that J_{0c} was < 0.5 fAcm^{-2} when we assume S_{int} = 0 cms^{-1}. Despite the higher tunnel barrier for holes than for electrons, the J_{0c} values for n-type and p-type are the same. Only at d < 1 nm we observed a significant increase in J_{0c} values for p+-poly up to 3 fAcm^{-2}, reflecting that the oxide barrier becomes more permeable for electrons.

The data in Fig. 3 also include values obtained with a more realistic S_{int} = 1000 cms^{-1}; the J_{0c} then essentially represents the J_{0p} already discussed above using the Girisch model. The increase in J_{0c} with oxide thickness d reflects the reduction of the field effect. This also determines the main difference between values for the p-type and n-type poly.

The thickness of the tunnel oxide is much more critical for the calculated values of ρ_c. Over the range 1-2

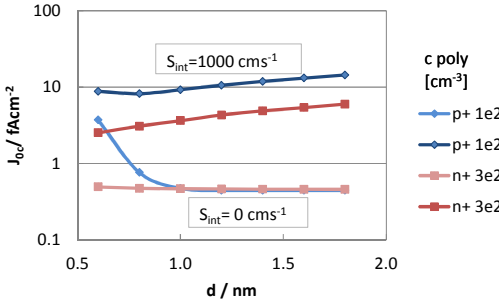

Figure 3: The recombination parameter J_{0c} of the metal/poly-Si/oxide/c-Si from Atlas simulations using the quantum-mechanical tunnel model as function of the oxide thickness d. The lines represent different polarity and values used for S_{int}.

nm these values change by 3-4 orders of magnitude (Fig. 4). Moreover, the different barrier for electron and holes now leads to very significant difference in ρ_c for p-type and n-type contacts. As pointed out by Peibst *et al.*, these features are at conflict with reported data for doped poly-Si/oxide layers [6,9,12] No strong correlation of ρ_c and oxide thickness d in the range 1-2 nm has been observed, nor a systematically larger resistance ρ_c for p+ poly-Si compared to n+ poly-Si [5-7,12]. Moreover, even for n+ poly-Si layers reported values of ρ_c are in the order 5-20 mΩcm^2 rather than the 0.1-1 Ωcm^2 consistent with a tunnel oxide [1,6,7,22]. It has also been reported that the presence of an in-diffusion tail reduces the ρ_c [11]; this is corroborated by the results in Fig. 4. But notice that these tails do not change the dependency on d, nor do they remove the very different tunnel permeability for holes and electrons.

According to recent analyses, in high efficiency cells ρ_c will be < 1 Ωcm^2 [9]. However, it has been recognized before that the oxide probably does not always behave like a perfect quantum-mechanical tunnel barrier. One cause can be that here are pin-holes in the oxide [6,12]; another reason can be that the tunnelling is assisted by the presence of traps in the oxide. Rather than to modify the parameters of the tunnel model or to extend the model, we now represent the oxide barrier by a thin (1.5 nm) layer of intrinsic silicon with an effective charge carrier mobility μ. Because the layer is so thin, the carrier density at either side of the layer determines the carrier density in the layer. By using the mobility of the charge

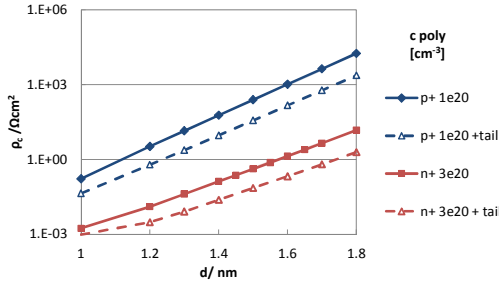

Figure 4: The area specific junction resistance ρ_c of the poly-Si/oxide/c-Si from Atlas simulations using the quantum-mechanical tunnel model as function of the oxide thickness d. The lines represent different polarity and levels of poly-Si dopant. The dashed lines were calculated using a gaussian in-diffusion tail with depth factor a=0.5 µm and N_s=1·10^{19} cm^{-3} for p+ and N_s=5·10^{19} cm^{-3} for n+, respectively.

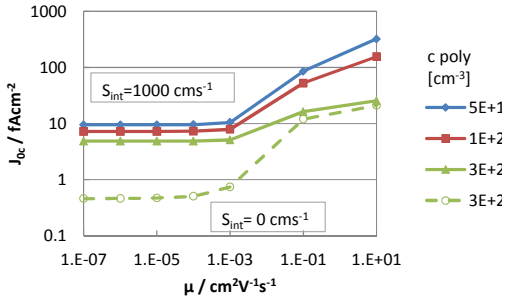

Figure 5: The recombination parameter J_{0c} of the metal/poly-Si/oxide/c-Si from Atlas simulations as function of the effective charge carrier mobility in the i-Si layer representing the oxide. The lines represent different levels of n+ poly-Si dopant.

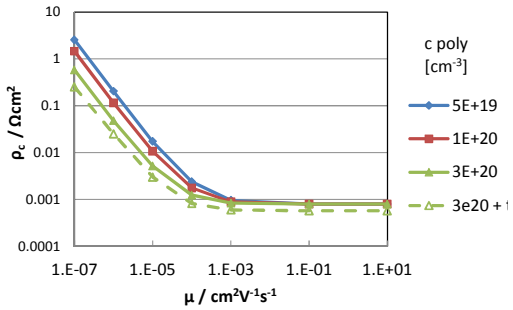

Figure 6: The area specific junction resistance ρ_c of the poly-Si/oxide/c-Si from Atlas simulations as function of the effective charge carrier mobility in the i-Si layer representing the oxide. The lines represent different levels of poly-Si dopant. The dashed line was calculated using a gaussian in-diffusion tail with depth factor 0.5 μm and N_s=5·10^{19} cm^{-3}.

carriers as a parameter, the conductivity of holes and electrons in the barrier layer can be further tuned, as is also the basis of a similar model proposed by Peibst *et al*. [6,9,12].

Fig.5 shows that using an effective charge carrier mobility < 10^{-3} Vcm^{-2}s^{-1} is as effective as a tunnel barrier in reducing J_{0c}. Note, that such mobility values are much smaller than in the poly-Si, or in doped crystalline silicon. The asymmetric conductivity of holes and electrons determines the selectivity, but due to the large driving force for minorities to the metal, where holes and electrons are at equilibrium, a low conductivity for minorities is needed to sufficiently suppress the minority transport to the contact [4].

At the high end of mobility values the J_{0c} is strongly dependent on the poly-dopant level as the minority concentration at the contact is now dominated by the dopant level and not by the barrier. Here, for clarity we only present results for the n+-poly layers. The results for p-type layers will only be different because of the different doping levels, and small differences in the band-bending between n+/n and p+/n systems resulting in different contributions of $J_{0p.}$ Note, that because of the expected low lifetime in poly-Si, the reduced charge carrier mobility is also instrumental in minimizing the recombination at the non-contacted area of poly-Si layers.

As expected the ρ_c as function of charge carrier mobility has the opposite trend, i.e. it strongly decreases with the mobility (Fig.6). By comparing data of Fig. 4 at 1.5 nm to Fig. 6 we can conclude that the quantum-mechanical tunnel mobility for electrons is in the order of < 10^{-6} cm^2 V^{-1}s^{-1} for electrons and even less for holes. But as Fig. 5 shows, such low values are not required for a low J_{0c}. The calculation of the maximum efficiency as function of the charge carrier mobility confirms this (Fig. 7). The range of mobility values that give the highest efficiency comprises a few orders of magnitude. Especially for p-type the calculated maximum efficiency can be much higher than predicted on the basis of the tunnel model.

The reduction of ρ_c due to the in-diffusion tail is also described using the model of effective charge carrier mobility. However, as Fig. 6 also shows, this effect is in absolute values not significant if the effective mobility is above the limit of the quantum-mechanical tunnel model.

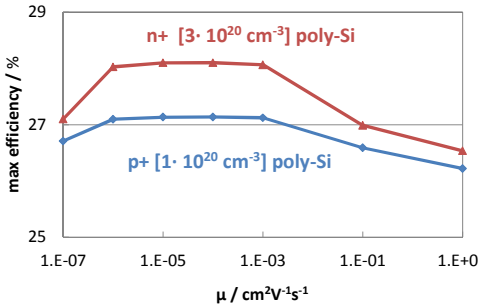

Figure 7: The calculated maximum efficiency that can be achieved using J_{0c} and ρ_c values with effective mobility charge carrier mobility μ in the i-Si layer representing the oxide.

3.3 Fire-through metallization

The bifacial n-type PERPoly (Passivated Emitter Rear PolySilicon) solar cells of ECN feature an n+-poly-Si layer at the rear. This n+-poly-Si layer is contacted by an industrial, screen-printed metallization pattern [23]. This configuration differs in two ways from the one depicted in Fig.1 and discussed in section 3.2 above. First, a large part of the poly-Si area is not contacted but covered by a SiN_x layer. However, due to the low lifetime in poly-Si the J_0 of this area will be similar to the J_{0c} of a metal covered area. Secondly, some of the metal will spike through the oxide, which would lead to J_0 values locally much higher than the J_{0c} calculated in section 3.2. The degree of spiking can to some extent be controlled by the poly-Si layer thickness, but the presence of in-diffusion tails can also effectively reduce the J_0 [24].

4 DISCUSSION

With the field provided by poly-layers with dopant concentrations ≥ 10^{20} cm^{-3}, a recombination velocity S_{int} = 1000 cms^{-1} at the oxide/c-Si interface is adequate to obtain J_{0c} < 10 fAcm^{-2} values. Such low values of S_{int} can be achieved by hydrogenation of the oxide/wafer interface, e.g. by deposition of SiN_x:H on the poly-Si and optional subsequent firing [3]. Since the oxide acts as a diffusion barrier, the dopant concentration in the poly can reach a uniform value close to the solubility limit over

the whole poly thickness. As this limit is higher for phosphorous than boron, the field effect of n-poly can be stronger. The less good passivation often observed for p-poly is at least in part due to a weaker field although also the oxide/c-Si interface may contain more defects because of the presence of boron ions.

The simulation results presented this paper show that the oxide has a significant role in providing good carrier selectivity for the contacts. Good carrier selectivity means that the transport of the majority carrier to the contact is unimpeded but the transport of minority carriers is efficiently suppressed. As discussed in 3.2 we found that treating the oxide as a perfect quantum mechanical tunnel barrier gives low J_{0c} values, but also large ρ_c values. Moreover, experimental data also suggest that the oxide is often very different from the ideal tunnel barrier because of e.g. dopants and pinholes etc. [6,10,12].

With the effective charge carrier mobility model more justice can be done to these differences. This model is easy to use with existing simulation software, and it retains the important function of the oxide in mechanism of the carrier selectivity, i.e. the reduction of the conductivity for carrier transport. By setting the effective mobility at values < 10^{-6} $cm^2V^{-1}s^{-1}$ the tunnel behaviour can be reproduced, including the effect of in-diffusion tails. But by using larger mobility values different behaviour of charge transport can be described, such as through pinholes or trap-assisted tunnelling. Using a Si layer with an effective charge carrier mobility is therefore an easy to implement and flexible way to represent the oxide layer in numerical simulations. The charge carrier mobility values can be derived from experimental values of the junction resistance ρ_c.

The simulation result that the maximum efficiency is not obtained for a perfect tunnel oxide but rather for an oxide more permeable for charge carriers seems favourable for the development of this type of contact layers. First of all it shows that p-contacts with low J_{0c} do not necessarily have a prohibitively large ρ_c. Secondly, oxides that are damaged by high temperature treatment, or contain large concentrations of dopant can still be good enough in the suppression of minority transport.

This observation, that the interfacial oxide does not necessarily have to be a perfect tunnel oxide, is also consistent with excellent passivation results obtained at ECN with “leaky” oxides [10], which have significant in-diffusion tails. Rather than destroying the selectivity, such tails can be beneficial in providing additional lateral conductivity in the case of non-full area contacts. This enables the use of thinner poly layers, and hence less optical losses. Moreover, in the case of fire-through contacts, when metal spikes through the interfacial oxide, such tails can provide extra shielding of the contact. However, in all cases the benefits of the tail have to outweigh the additional Auger recombination.

5 CONCLUSIONS

The interfacial oxide plays an essential role both for the passivating properties and for the carrier selectiveness of poly-Si/oxide contact layers. As during processing the oxide is a diffusion barrier, high dopant levels close the solubility level are achieved, which provide a large field effect in the wafer. Hydrogenation is still required but with known oxides the interface properties provide excellent wafer passivation.

We proposed an intrinsic thin (1.5 nm) silicon layer with a low effective charge carrier mobility as a good representation of the oxide as barrier for charge carriers. The simulations showed that this barrier function is essential for the carrier selectivity, i.e. a charge carrier mobility much smaller than found in doped c–Si is consistent with low J_{0c} values. Too high values obviously impede the majority transport too much; the optimum value for the effective mobility through the barrier is not as low as would correspond to tunnel model.

The proposed method to represent the oxide in simulations is not only convenient and easy to implement, it also seems better suited to represent the oxide in simulations especially in the case of p+-type layers and for more “leaky oxides” with large in-diffusion tails. This enables a more realistic study of the benefits of these in-diffusion tails in reducing the junction resistance, providing lateral conductivity or contact shielding in the case of fire-through metallization.

REFERENCES

[1] F. Feldmann, M. Bivour, C. Reichel, M. Hermle, and S. W. Glunz, Solar Energy Materials and Solar Cells 120, Part A (2014) 270-274.
[2] U. Romer, R. Peibst, T. Ohrdes, B. Lim, J. Krugener, T. Wietler, and R. Brendel, IEEE Journal of Photovoltaics 5 (2015) 507.
[3] M. K. Stodolny, M. Lenes, Y. Wu, G. J. M. Janssen, I. G. Romijn, J. R. M. Luchies, and L. J. Geerligs, Solar Energy Materials and Solar Cells 158, Part 1 (2016) 24-28.
[4] U. Würfel, A. Cuevas, and P. Würfel, IEEE Journal of Photovoltaics 5 (2015) 461-469.
[5] D. Yan, A. Cuevas, Y. Wan, and J. Bullock, Solar Energy Materials and Solar Cells 152 (2016) 73-79.
[6] R. Peibst, U. Römer, Y. Larionova, M. Rienäcker, A. Merkle, N. Folchert, S. Reiter, M. Turcu, B. Min, J. Krügener, D. Tetzlaff, E. Bugiel, T. Wietler, and R. Brendel, Solar Energy Materials and Solar Cells 158 (2016) 60-67.
[7] D. Yan, A. Cuevas, J. Bullock, Y. Wan, and C. Samundsett, Solar Energy Materials and Solar Cells (2015)
[8] H. Steinkemper, B. Michl, M. Hermle, and S. W. Glunz, Energy Procedia 92 (2016) 225-231.
[9] R. Brendel and R. Peibst, IEEE Journal of Photovoltaics 6 (2016) 1413-1420.
[10] M. K. Stodolny, J. Anker, L. J. Geerligs, G. J. M. Janssen, B. W. H. van de Loo, J. Melskens, O. Isabella, J. Schmitz, M. Lenes, J. M. Luchies, W. M. M. Kessels, and I. G. Romijn, Energy Proc. (2017) in press.
[11] H. Steinkemper, F. Feldmann, M. Bivour, and M. Hermle, Energy Procedia 77 (2015) 195.
[12] R. Peibst, U. Römer, K. R. Hofmann, B. Lim, T. F. Wietler, J. Krügener, N. P. Harder, and R. Brendel, IEEE Journal of Photovoltaics 4 (2014) 841-850.
[13] R. B. M. Girisch, R. P. Mertens, and R. F. De Keersmaecker, IEEE Transactions on Electron Devices 35 (1988) 203.
[14] L. E. Black and K. R. McIntosh, IEEE Journal of Photovoltaics 3 (2013) 936-943.
[15] Atlas, www.silvaco.com, (2013).
[16] P. Altermatt, Journal of Computational Electronics 10 (2011) 314-330.

[17] A. Schenk, J.Appl.Phys. 84 (1998) 3684-3695.
[18] R. Sinton and D. Macdonald, *WCT-120 Photoconductance Lifetime Tester and optional Suns-VOC Stage User Manual*, Sinton Consulting, Inc, Boulder, Colorado, 2006.
[19] A. Fell, IEEE Transactions on Electric Devices 60 (2013) 733-738.
[20] A. Richter, J. Benick, F. Feldmann, A. Fell, M. Hermle, and S. W. Glunz, Solar Energy Materials and Solar Cells (2017) in press.
[21] H. Steinkemper, F. Feldmann, M. Bivour, and M. Hermle, IEEE Journal of Photovoltaics 5 (2015) 1348-1356.
[22] M. Rienäcker, M. Bossmeyer, A. Merkle, U. Römer, F. Haase, J. Krügener, R. Brendel, and R. Peibst, IEEE Journal of Photovoltaics 7 (2017) 11-18.
[23] M. K. Stodolny, M. Lenes, Y. Wu, G. J. M. Janssen, I. G. Romijn, J. R. M. Luchies, and L. J. Geerligs, Solar Energy Materials and Solar Cells 158, Part 1 (2016) 24-28.
[24] M. K. Stodolny, L. J. Geerligs, G. J. M. Janssen, R. van de Sanden, J. Melskens, R. Santbergen, O. Isabella, M. Lenes, J. M. Luchies, W. M. M. Kessels, and I. G. Romijn, 33rd EUPVSEC, Amsterdam (2017).